Ionics
DOI 10.1007/s11581-014-1213-1

ORIGINAL PAPER

Electrospun preparation and lithium storage properties of $NiFe_2O_4$ nanofibers

Lei Luo · Rongrong Cui · Ke Liu · Hui Qiao · Qufu Wei

Received: 16 May 2014 / Revised: 15 July 2014 / Accepted: 20 July 2014

Abstract In this paper, we successfully synthesized $NiFe_2O_4$ nanofibers via simple electrospinning process followed by calcination process. Only peaks of $NiFe_2O_4$ could be observed from X-ray diffractometry patterns, indicating the formation of pure compound. Scanning electron microscope and transmission electron microscopy images showed the as-spun $NiFe_2O_4$ nanofibers calcined at 800 °C ranged from 130 to 220 nm in diameter. The electrochemical properties of the nanofibers anode material for lithium-ion batteries were tested. It was found that the obtained $NiFe_2O_4$ nanofibers calcined at 800 °C possessed higher reversible capacity and cycling stability than that of the samples calcined at 600 °C. The as-prepared $NiFe_2O_4$ nanofibers calcined at 800 °C exhibited a high initial discharge capacity of 1,304 mAh g^{-1} in the potential range of 3.0–0.01 V, and the stabilized capacity was as high as 514 mAh g^{-1} after 60 cycles. Moreover, the as-prepared $NiFe_2O_4$ nanofibers calcined at 800 °C also exhibited high capacity at higher charge/discharge rate.

Keywords Electrospinning · $NiFe_2O_4$ nanofibers · Anode · Lithium-ion batteries

Introduction

Owing to the advantages of less weight, high-energy density, high-operating voltage, and no "memory effect", lithium-ion batteries have attracted wide attention [1]. Anode material is an important factor in determining capacity and cycle life performance in lithium-ion batteries. Over the past decades, carbon, such as graphite, was the most utilized anode material for lithium-ion batteries attributing to the low cost, long cycle life, and low working potential [2, 3]. However, commercial carbon materials only have a relatively low specific capacity (372 mAh g^{-1}). Hence, it is necessary to develop a kind of novel anode material to substitute conventional carbon materials.

Much attention has been recently focused on nanostructured transition metal oxides because of their high capacities, which was nearly two or three times higher than that of commercial carbon materials [4–14]. Their high recharging rates and great capacity retention were also demonstrated. Li reported that the discharge capacity of the three-dimensional-ordered macroporous $CoFe_2O_4$ stabilized at about 700 mAh g^{-1} after 30 cycles [15]. Nanostructured $ZnFe_2O_4$ powders, prepared by Ding et al., could reach an initial discharge capacity of 1,419.6 mAh g^{-1} [16]. MFe_2O_4 (M=Cu, Ni, Co) thin film electrodes synthesized by an electrochemical route delivered a reversible capacity of 450–460 mAh g^{-1} [17]. Liu et al. showed that $NiFe_2O_4$ powders prepared by a novel low-temperature route possessed the initial discharge capacity of up to 1,400 mAh g^{-1} [18]. During the last decade, MFe_2O_4 nanofibers synthesized by a facile electrospinning process have been widely reported, and their magnetic properties were studied [19–22]. However, as far as we are concerned, those electrospun MFe_2O_4 nanofibers used as anode materials in lithium-ion battery are rarely reported.

In this work, we prepared $NiFe_2O_4$ nanofibers via electrospinning process in combination with calcination. Only peaks of $NiFe_2O_4$ could be observed from X-ray

L. Luo · R. Cui (✉) · H. Qiao (✉) · Q. Wei
Key Laboratory of Eco-Textiles, Ministry of Education, Jiangnan University, Wuxi, Jiangsu 214122, China
e-mail: cuirong3243@sina.com
e-mail: huiqiaoz@163.com

K. Liu
Hubei Key Laboratory of Low Dimensional Optoelectronic Material and Devices, Hubei University of Arts and Science, Xiangyang, Hubei 441053, China

Published online: 13 August 2014

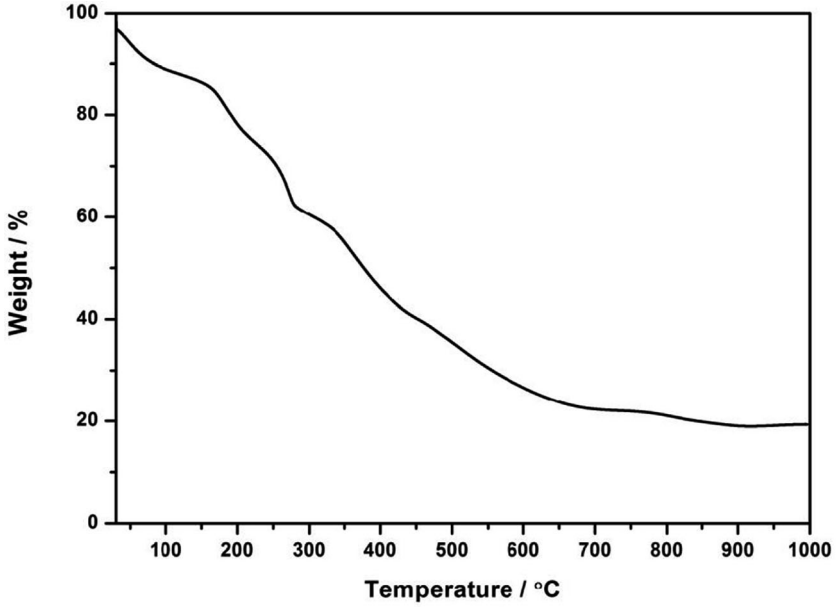

Fig. 1 TG curve of the as-prepared PVP/$Ni(CH_3COO)_2 \cdot 4H_2O$/$Fe(NO_3)_3 \cdot 9H_2O$ composite nanofibers

diffractometry patterns indicating the formation of pure compound. Scanning electron microscope and transmission electron microscopy images showed the as-spun $NiFe_2O_4$ nanofibers calcined at 800 °C ranged from 130 to 220 nm in diameter. The as-prepared $NiFe_2O_4$ nanofibers calcined at 800 °C exhibited a high initial discharge capacity of 1,304 mAh g^{-1} in the potential range of 3.0–0.01 V, and the stabilized capacity was as high as 514 mAh g^{-1} after 60 cycles. Moreover, the as-prepared $NiFe_2O_4$ nanofibers calcined at 800 °C also exhibited high capacity at higher charge/discharge rate.

Experimental section

Material preparation

In the preparation of the solution, $Ni(CH_3COO)_2 \cdot 4H_2O$ and $Fe(NO_3)_3 \cdot 9H_2O$ with a molar rate of 1:2 were dissolved in DMF (10 mL), followed by stirring until the complete dissolution of the solid reagents. A PVP/ethanol solution was prepared by dissolving 2.0 g PVP to 18 mL ethanol and stirred for 5 h. Subsequently, the former was added slowly to the later under vigorous stirring for 12 h at room temperature to form a

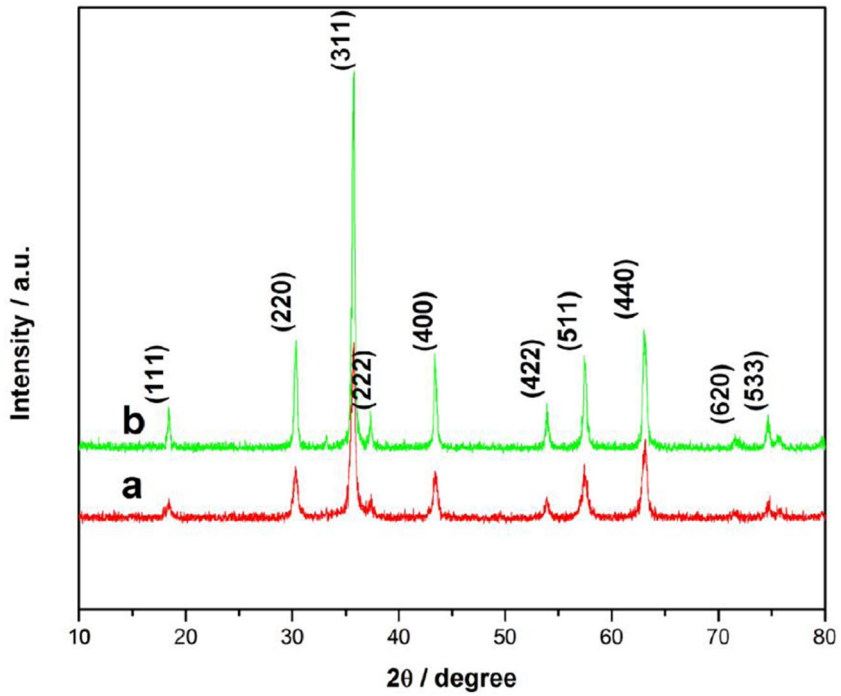

Fig. 2 XRD patterns of the as-prepared $NiFe_2O_4$ nanofibers obtained at 600 °C (**a**) and 800 °C (**b**)

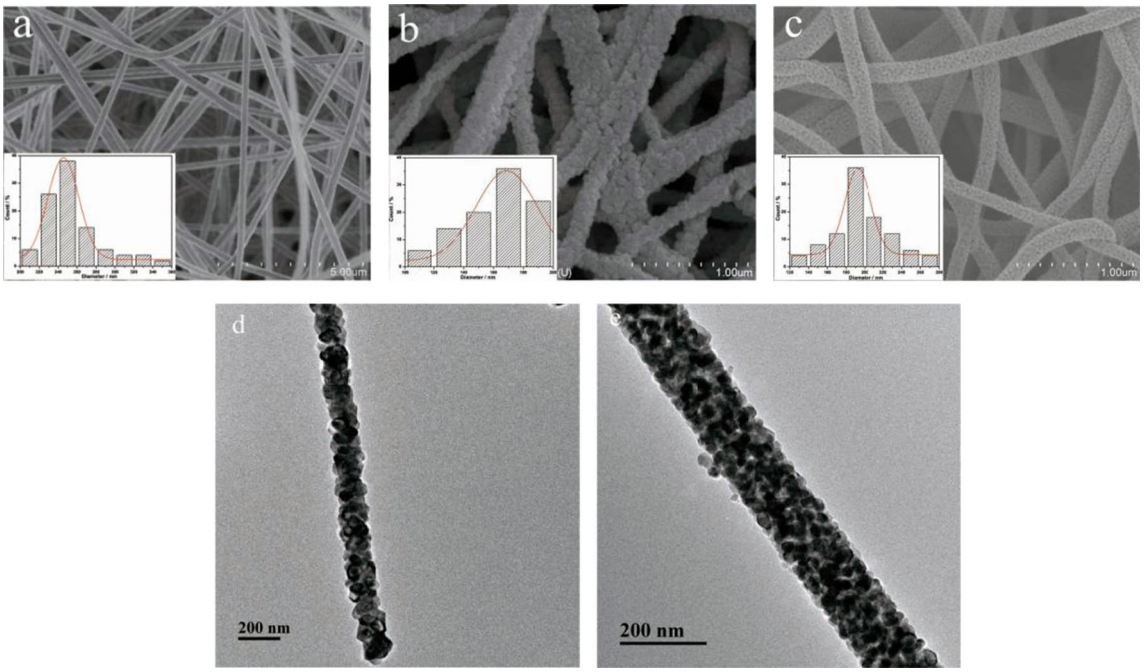

Fig. 3 SEM images of the as-prepared PVP/$Ni(CH_3COO)_2 \cdot 4H_2O$/$Fe(NO_3)_3 \cdot 9H_2O$ composite nanofibers (**a**) and $NiFe_2O_4$ nanofibers obtained at 800 °C (**b**) and 600 °C (**c**); TEM images of $NiFe_2O_4$ nanofibers obtained at 800 °C (**d**) and 600 °C (**e**)

uniform solution. The final solution was used for electrospinning.

The precursor solution was loaded into a 20-mL plastic syringe having a blunt-end stainless-steel needle with inside diameter of 0.41 mm. The electrospinning setup included a high-voltage power supply and a nanofiber collector of electrically grounded aluminum foil that covered a laboratory-produced roller. A positive voltage of 15 kV was applied between the needle tip and grounded aluminum foil collector with a distance of 15 cm. The solution was fed at a constant rate of 0.3 mL/h using a syringe pump. The electrospinning was performed in an open environment at room temperature.

The obtained composite nanofibers mats were then calcined in air atmosphere for 5 h at 600 and 800 °C, respectively, with a heating rate of 1 °C/min yielding the $NiFe_2O_4$ nanofibers.

Material characterization

The morphologies of the as-prepared PVP/$NiFe_2O_4$ composite nanofibers and $NiFe_2O_4$ nanofibers were observed using a Hitachi S4800 field emission scanning electron microscopy (FE-SEM). Prior to FE-SEM examination, the nanofibers were sputter coated with gold to avoid charge accumulations. Transmission electron microscopy (TEM) was performed on a JEOL JEM-2100 transmission electron microscopy unit at an accelerating voltage of 120 kV. The samples for TEM were prepared by dispersing the final powders in ethanol, the dispersion was then dropped on carbon-copper grids. X-ray powder diffraction patterns were obtained to observe the crystal structure of the $NiFe_2O_4$, using Bruker D8 Advance X-ray Diffractometer using Cu-Kα irradiation (λ=1.5406 Å) over Bragg angles from 10° to 80° with the scanning speed of 4°/min. Thermogravimetric analysis (TGA) was conducted on a TGA 2050 analyzer under an air flow of 50 mL/min with a heating rate of 10 °C/min from room temperature to 1,000 °C. The nitrogen absorption and desorption isotherms at 77 K were measured using Micrometrics ASAP2020 system after samples were vacuum dried at 180 °C overnight, and the specific surface area and the pore size distribution were calculated using the Brunauer-Emmett-Teller (BET) and Barrett-Joyner-Halenda (BJH) methods, respectively.

Electrochemical measurements

Electrodes were prepared by mixing active materials (80 wt%), carbon black (10 wt%), and poly(tetrafluoroethylene) (10 wt%) with 2-propanol to form a paste. The paste was then roll-pressed into 0.17-mm thick film and dried at 100 °C for 12 h. Finally, the paste was coated onto a nickel net. Prior to cell assembling, the electrodes with an area of 0.64 cm^2 were dried at 120 °C for 4 h. The testing cells had a typical three-electrode construction using lithium foils as both counter electrode and reference electrode, Celgard 2300 membrane as the separator, and 1 M $LiPF_6$ dissolved in ethylene carbonate (EC), dimethyl carbonate (DMC), and ethylene methyl carbonate (EMC) (1:1:1, *v*/*v*/*v*) as the electrolyte. The cells were assembled in an argon-filled glove box. The galvanostatic charge/discharge tests were carried out at a constant current density of 50 mA g^{-1} in a range

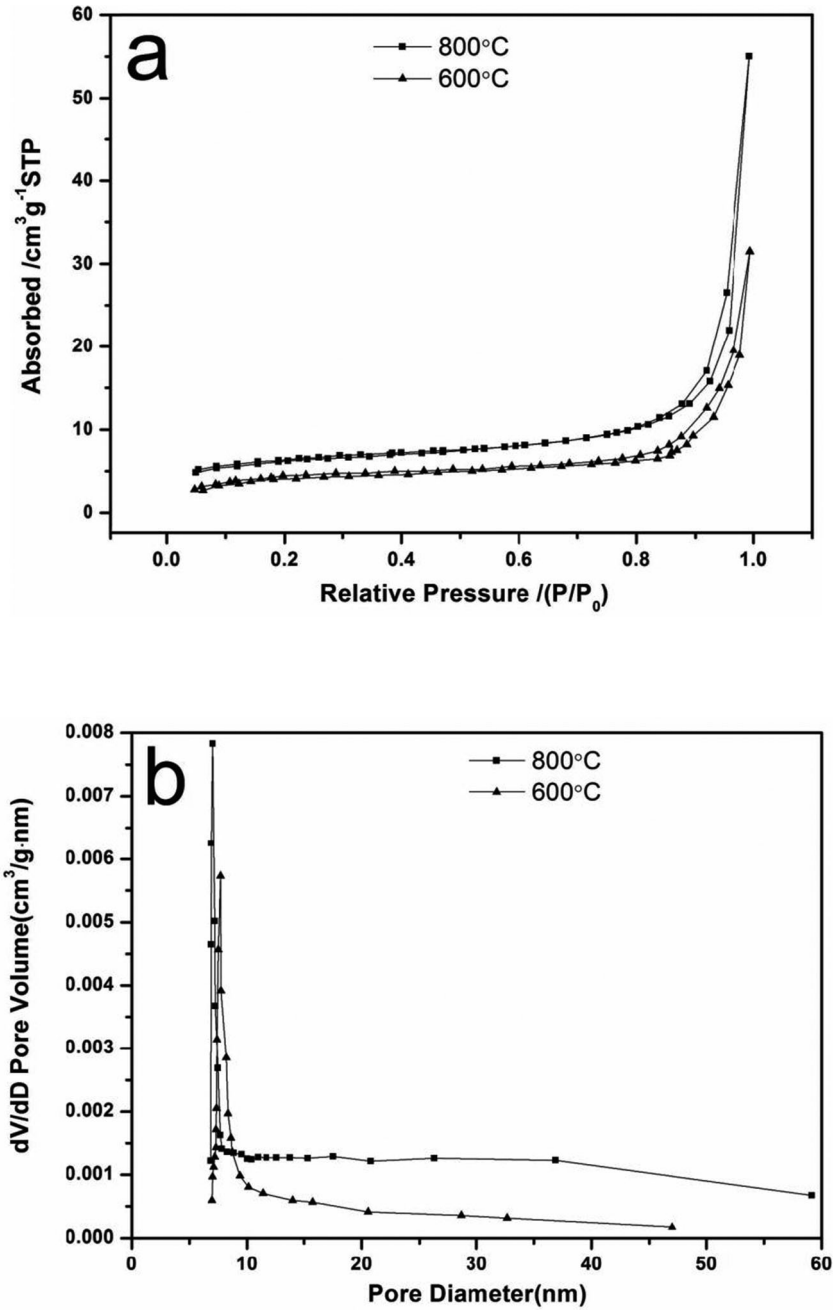

Fig. 4 Nitrogen adsorption-desorption isotherm (**a**) and pore size distribution curve (**b**) of the $NiFe_2O_4$ nanofibers obtained at 800 and 600 °C

of 3.0–0.01 V (versus Li/Li^+) on a Neware battery tester. All the tests were performed at room temperature.

Results and discussions

Figure 1 shows TG curve of the as-prepared PVP/$Ni(CH_3COO)_2 \cdot 4H_2O/Fe(NO_3)_3 \cdot 9H_2O$ composite nanofibers prepared by electrospinning technology. It can be seen that three steps of weight loss were found in the decomposition curve of the as-prepared PVP/$Ni(CH_3COO)_2 \cdot 4H_2O/Fe(NO_3)_3 \cdot 9H_2O$ composite nanofibers. The first step occurred from 30 up to about 160 °C, the weight loss in this step was approximately 14.4 %, attributing to the evaporation of physically absorbed water and residual solvent (ethanol and DMF) in the samples. In the second step, a weight loss took place from 160 to about 277 °C; the weight loss in this step was approximately 22.8 %, due to the partial combustion of organic PVP matrix and decomposition of Fe nitrates and Ni acetates accompanied by the release of carbon dioxide and water molecule (the organic PVP matrix decomposed into carbon dioxide and the lost of crystal water in Fe nitrates and Ni acetates). The TG curve also shows a major weight loss step from 277 to 700 °C, the weight loss achieved 40.5 % because of the completely decomposition

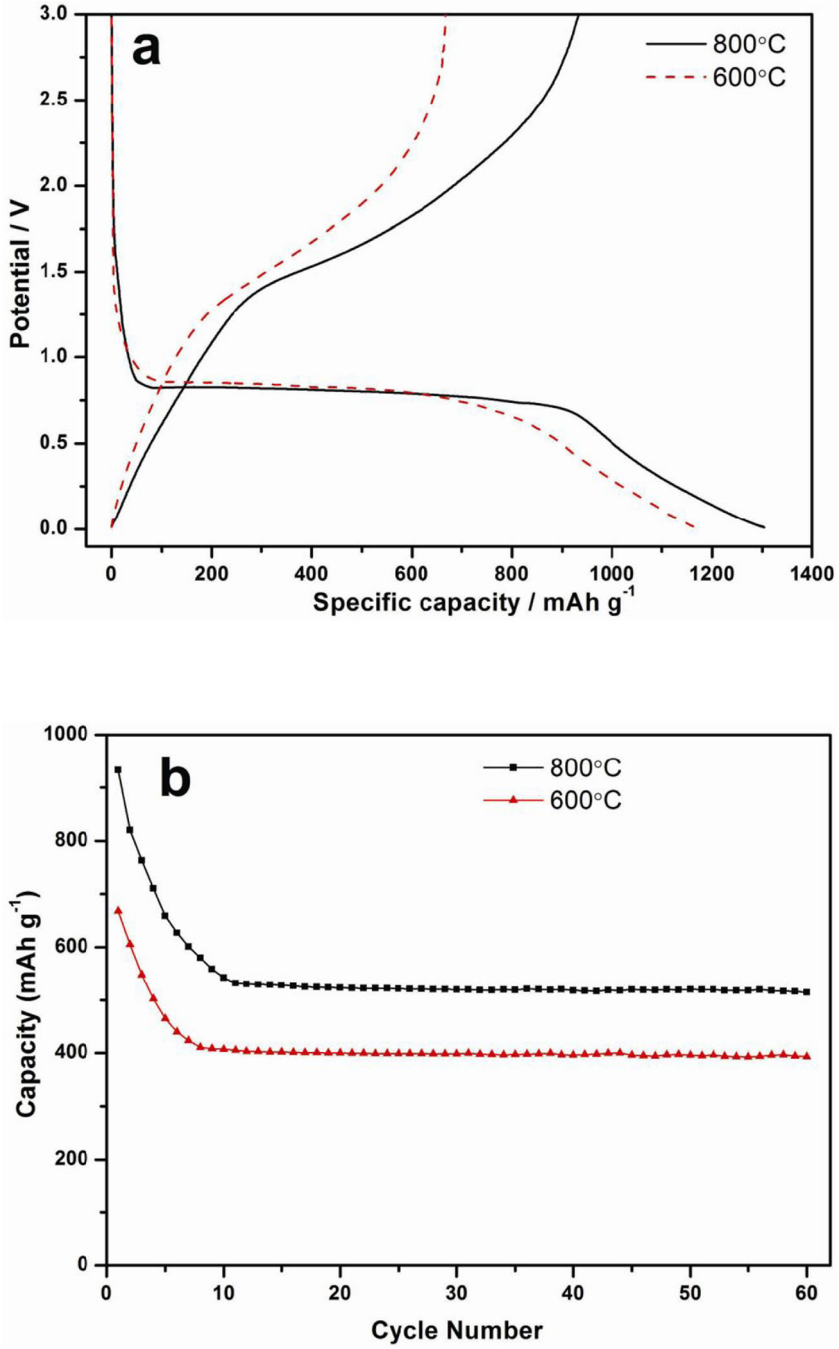

Fig. 5 Initial discharge/charge curves (**a**) and cyclic performances (**b**) of the $NiFe_2O_4$ nanofibers electrodes calcined at 800 and 600 °C

of PVP, Fe nitrates, and Ni acetates. In this step, Fe nitrates and Ni acetates decomposed into iron oxide and nickel oxide, respectively, and then these two metal oxides formed into $NiFe_2O_4$. When the temperature constantly increased up to 1,000 °C, no weight loss was observed on the TG curve, indicating the formation of crystalline $NiFe_2O_4$ as the final products.

The crystal structures of the resulting products were examined by X-ray diffractometry (XRD). Figure 2 shows the XRD patterns of the as-prepared $NiFe_2O_4$ nanofibers obtained at 600 and 800 °C for 5 h in air atmosphere, respectively. Obviously, calcination temperature affected the crystallization of resulting products. The peaks became sharper and the intensity increased with the increase of calcination temperature. After the products were calcined at 800 °C, the crystallinity of the resulting product has been improved significantly. All the diffraction peaks can well be indexed to the standard cubic $NiFe_2O_4$ structure with an Fm-3 m (227) space group (JCPDS File No. 86-2267). No peaks of any other phases or impurities could be observed, which confirmed the formation of pure compound. The diffraction peaks at $2\theta=18.428°$, 30.309°, 35.701°, 37.320°, 43.383°, 53.814°, 57.393°,

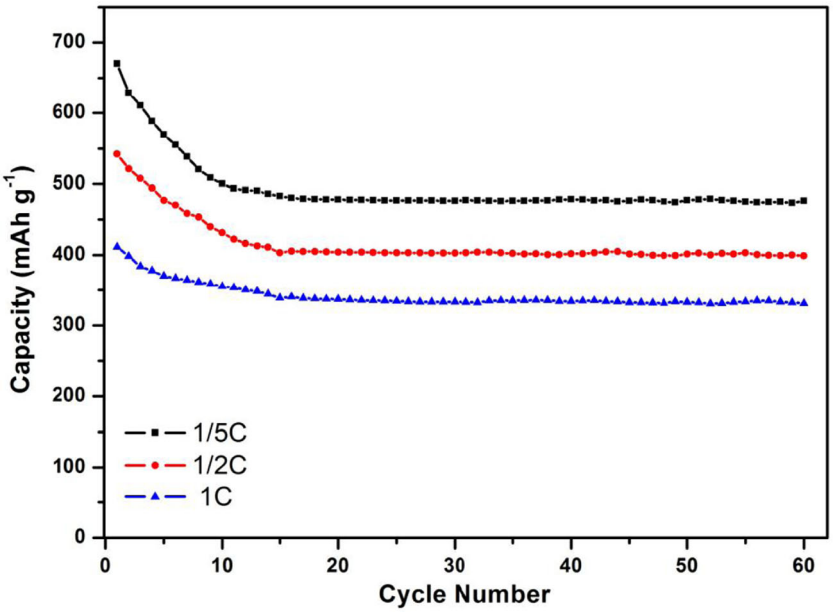

Fig. 6 Rate capability of the $NiFe_2O_4$ nanofibers electrode calcined at 800 °C

63.021°, 71.490°, and 74.561° corresponded to (*hkl*)=(111), (220), (311), (222), (400), (422), (511), (440), (620), and (533) reflections, respectively. The lattice parameters of $NiFe_2O_4$ phase were calculated to be $a=b=c=8.337$ Å and $\alpha=\beta°=°\gamma°=°90°$, which are consistent with the literature values [23]. According to Scherrer's equation, $D=\kappa\lambda/\beta_{1/2}\cos\theta$, the average sizes of the $NiFe_2O_4$ particles were 20.5 and 30.6 nm corresponding to 600 and 800 °C, respectively. These results revealed that grain sizes of the products became larger with the increase of calcination temperature.

The morphologies of the as-prepared PVP/$Ni(CH_3COO)_2\cdot 4H_2O$/$Fe(NO_3)_3\cdot 9H_2O$ composite nanofibers and $NiFe_2O_4$ nanofibers obtained after calcination are shown in Fig. 3. From Fig. 3a, it was clearly observed that the as-prepared composite nanofibers formed a continuous fibrous structure, and the average diameter was 250 nm. However, the average diameters of the as-prepared $NiFe_2O_4$ nanofibers after calcining decreased from 190 nm for 600 °C to 170 nm for 800 °C (Fig. 3b, c). The reduction in diameter of $NiFe_2O_4$ nanofibers could be ascribed to the removal of PVP and the decomposition of metal salts. The $NiFe_2O_4$ nanofibers were composed of packed particles or crystallites. According to literatures, the changes that occurred in the morphology above are connected to a dramatic change in crystal structure [21, 22]. The detailed morphology and structure of the PVP/$NiFe_2O_4$ composite nanofibers calcined at 800 and 600 °C were further investigated by TEM. As shown in Fig. 3d, e, it was obvious that $NiFe_2O_4$ nanoparticles which composed $NiFe_2O_4$ nanofibers grew larger with the increase of calcination temperature, and their surfaces became rough. It also could be seen that $NiFe_2O_4$ nanoparticles piled compactly along fiber orientation with the increase of calcination temperature.

The (a) nitrogen adsorption-desorption isotherm and (b) pore size distribution curve of $NiFe_2O_4$ nanofibers calcined at 800 and 600 °C were presented in Fig. 4. The isotherm belonged to type IV according to IUPAC classification, which was a typical characteristic adsorption-desorption isotherm of mesoporous materials with hysteresis loops at a high partial pressures [24]. The BET surface area was increased from 23.5 $m^2\ g^{-1}$ for $NiFe_2O_4$ nanofibers obtained at 600 °C to 35.9 $m^2\ g^{-1}$ for $NiFe_2O_4$ nanofibers obtained at 800 °C. The average pore diameter was decreased from 7.5 to 7.0 nm, respectively. The large pore sizes of $NiFe_2O_4$ nanofibers were favorable for the diffusion of the electrolyte rendering better Li^+ ion transfer [25, 26].

The (a) initial discharge/charge curves and (b) cycle performances of the $NiFe_2O_4$ nanofibers electrodes calcined at 800 and 600 °C are shown in Fig. 5. As shown in Fig. 5a, the first discharge and charge curves of the as-prepared $NiFe_2O_4$ nanofibers electrodes exhibit voltage plateaus at around 0.8 and 1.4 V, respectively, corresponding to reduction/oxidation reactions during lithium insertion/extraction. The electrochemical reversible reaction can be expressed as follow [18, 27]:

$$NiFe_2O_4 + 8e^- + 8Li^+ \rightarrow Ni + 2Fe + 4Li_2O$$
$$Ni + 2Fe + 4Li_2O \leftrightarrow NiO + Fe_2O_3 + 8Li^+ + 8e^-$$

According to the reaction, eight lithium-ions were reversibly inserted and extracted, a specific reversible capacity of 915 mAh g^{-1} can be obtained. In fact, the first discharge capacity of the $NiFe_2O_4$ nanofibers electrodes calcined at 800 and 600 °C were about 1,304 and 1,166 mAh g^{-1}, respectively, which was much higher than the theoretical value. The extra capacity could be related to the formation of solid

electrolyte interphase (SEI) at the electrode/electrolyte interface caused by the reduction of electrolyte during the discharge process. The SEI played an important role in the process as it could be partially decomposed for the catalytic activity of Ni and Fe. The partially reversible formation/decomposition of the SEI would lead to an extra capacity of the cell [23, 28]. The first charge capacity of the $NiFe_2O_4$ nanofibers electrodes calcined at 800 °C was 933 mAh g^{-1}, which was higher than that of the electrodes calcined at 600 °C (668 mAh g^{-1}). The coulombic efficiency of the $NiFe_2O_4$ nanofibers electrodes calcined at 600 and 800 °C were 57.3 and 71.5 %, respectively. The large irreversible capacity loss of the $NiFe_2O_4$ nanofibers electrodes may be attributed to the irreversible decomposition of the SEI during charging together with the incomplete conversion reaction [2, 29, 30].

From Fig. 5b, we can clearly see that the capacity decreased with the increase of the cycle numbers, and it can reach a relatively stable reversible capacity only after 10 cycles. The specific capacity after 60 cycles for the $NiFe_2O_4$ nanofibers electrodes calcined at 800 °C was 514 mAh g^{-1}, which was much higher than that of the electrodes calcined at 600 °C (393 mAh g^{-1}). The improvement of electrochemical performance of the samples calcined at 800 °C was possibly caused by the higher crystallization, resulting in the reduction of the lattice defects, which facilitates the lithium-ions' insertion and extraction [11].

Figure 6 was the rate capability of the $NiFe_2O_4$ nanofibers electrode calcined at 800 °C. The as-prepared samples calcined at 800 °C exhibited high capacity at higher charge/discharge rate. The charge capacities of 670, 542, and 411 mAh g^{-1} were obtained at the current density of C/5, C/2, and 1C rates, respectively. The charge capacity fell off with the increase of charge/discharge current density because when the current was increased, the diffusion rate of lithium-ions was lower than that of the anode reaction, which led to the incomplete diffusion of lithium-ions and the structure collapse [18].

Conclusions

In this study, we successfully synthesized $NiFe_2O_4$ nanofibers via simple electrospinning process followed by calcination process. It was found that the obtained $NiFe_2O_4$ nanofibers calcined at 800 °C possessed higher reversible capacity and cycling stability than that of the samples calcined at 600 °C. The as-prepared $NiFe_2O_4$ nanofibers calcined at 800 °C exhibited a high initial discharge capacity of 1,304 mAh g^{-1}, and the stabilized capacity was as high as 514 mAh g^{-1} after 60 cycles. Moreover, the as-prepared $NiFe_2O_4$ nanofibers calcined at 800 °C also exhibited high capacity at higher charge/discharge rate. The excellent electrochemical performances make $NiFe_2O_4$ nanofibers a promising anode material for lithium-ion batteries in the future.

Acknowledgments This work was financially supported by the National Natural Science Foundation of China (21201083), Cooperative Innovation Fund-Prospective Project of Jiangsu Province (BY2014023-29 and BY2014023-23), Hubei Key Laboratory of Low Dimensional Optoelectronic Material and Devices (13XKL01002), the open project program of Key Laboratory of Eco-textiles, Ministry of Education, Jiangnan University (KLET1106 and KLET1301), the National High-tech R&D Program of China (863 Program) (2012AA030313), and the Innovation Program for Graduate Education in Jiangsu Province (KYLX_1135 and SJLX_0525).

References

1. Sui J, Zhang C, Hong D, Li J, Cheng Q, Li ZG, Cai W (2012) Facile synthesis of MWCNT-$ZnFe_2O_4$ nanocomposites as anode materials for lithium ion batteries. J Mater Chem 22:13674–13681
2. Qiao H, Li J, Fu JP, Kumar D, Wei QF, Cai YB, Huang FL (2011) Sonochemical synthesis of ordered SnO_2/CMK-3 nanocomposites and their lithium storage properties. ACS Appl Mater Interfaces 3:3704–3708
3. Camean I, Garcia AB (2011) Graphite materials prepared by HTT of unburned carbon from coal combustion fly ashes: performance as anodes in lithium-ion batteries. J Power Sources 196:4816–4820
4. Poizot P, Laruelle S, Grugeon S, Dupont L, Tarascon JM (2000) Nano-sized transition-metal oxides as negative-electrode material for lithium-ion batteries. Nature 407:496–499
5. Poizot P, Laruelle S, Grugeon S, Dupont L, Tarasco JM (2001) Searching for new anode materials for the Li-ion technology: time to deviate from the usual path. J Power Sources 97–98:235–239
6. Wang Y, Su DW, Ung A, Ahn JH, Wang GX (2012) Hollow $CoFe_2O_4$ nanospheres as a high capacity anode material for lithium ion batteries. Nanotechnology 23:055402
7. Wang Y, Park J, Sun B, Ahn H, Wang GX (2012) Wintersweet-flower-like $CoFe_2O_4$/MWCNTs hybrid material for high-capacity reversible lithium storage. Chem Asian J 7:1940–1946
8. Hwa Y, Sung JH, Wang B, Park CM, Sohn HJ (2012) Nanostructured Zn-based composite anodes for rechargeable Li-ion batteries. J Mater Chem 22:12767–12773
9. Yang YY, Zhao YQ, Xiao LF, Zhang LZ (2008) Nanocrystalline $ZnMn_2O_4$ as a novel lithium-storage material. Electrochem Commun 10:1117–1120
10. Chu YQ, Fu ZW, Qin QZ (2004) Cobalt ferrite thin films as anode material for lithium ion batteries. Electrochim Acta 49:4915–4921
11. Qiao H, Luo QH, Fu JP, Li J, Kumar D, Cai YB, Huang FL, Wei QF (2012) Solvothermal preparation and lithium storage properties of Fe_2O_3/C hybrid microspheres. J Alloys Compd 513:220–223
12. Qiao H, Xiao LF, Zheng Z, Liu HW, Jia FL, Zhang LZ (2008) One-pot synthesis of CoO/C hybrid microspheres as anode materials for lithium-ion batteries. J Power Sources 185:486–491
13. Guo XW, Lu X, Fang XP, Mao Y, Wang ZX, Chen LQ, Xu XX, Yang H, Liu YN (2010) Lithium storage in hollow spherical $ZnFe_2O_4$ as anode materials for lithium ion batteries. Electrochem Commun 12:847–850
14. Deng YF, Zhang QM, Tang SD, Zhang LT, Deng SG, Shi ZC, Chen GH (2011) One-pot synthesis of $ZnFe_2O_4$/C hollow spheres as superior anode materials for lithium ion batteries. Chem Commun 47:6828–6830

15. Li ZH, Zhao TP, Zhan XY, Gao DS, Xiao QZ, Lei GT (2010) High capacity three-dimensional ordered macroporous $CoFe_2O_4$ as anode material for lithium ion batteries. Electrochim Acta 55:4594–4598
16. Ding Y, Yang YF, Shao HX (2011) High capacity $ZnFe_2O_4$ anode material for lithium ion batteries. Electrochim Acta 56:9433–9438
17. NuLi YN, Qin QZ (2005) Nanocrystalline transition metal ferrite thin films prepared by an electrochemical route for Li-ion batteries. J Power Sources 142:292–297
18. Liu HW, Zhu H, Yang HM (2013) A low temperature synthesis of nanocrystalline spinel $NiFe_2O_4$ and its electrochemical performance as anode of lithium-ion batteries. Mater Res Bull 48:1587–1592
19. Li D, Herricks T, Xia YN (2003) Magnetic nanofibers of nickel ferrite prepared by electrospinning. Appl Phys Lett 83:4586–4588
20. Zhao JX, Cheng YL, Yan XB, Sun DF, Zhu FL, Xue QJ (2012) Magnetic and electrochemical properties of $CuFe_2O_4$ hollow fibers fabricated by simple electrospinning and direct annealing. CrystEngComm 14:5879–5885
21. Ponhan W, Maensiri S (2009) Fabrication and magnetic properties of electrospun copper ferrite ($CuFe_2O_4$) nanofibers. Solid State Sci 11: 479–484
22. Maensiri S, Sangmanee M (2009) Magnesium ferrite ($MgFe_2O_4$) nanostructures fabricated by electrospinning. Nanoscale Res Lett 4: 221–228
23. Zhao HX, Zheng Z, Wong KW, Wang SM, Huang BJ, Li DP (2007) Fabrication and electrochemical performance of nickel ferrite nanoparticles as anode material in lithium ion batteries. Electrochem Commun 9:2606–2610
24. Sing KSW, Everett DH, Haul RAW, Moscou L, Pierotti RA, Rouquerol J, Siemieniewska T (1985) Reporting physisorption data for gas/solid systems with special reference to the determination of surface area and porosity. Pure Appl Chem 57:603–619
25. Wu LJ, Xiao QZ, Li ZH, Lei GT, Zhang P, Wang L (2012) $CoFe_2O_4$/C composite fibers as anode materials for lithium-ion batteries with stable and high electrochemical performance. Solid State Ionics 215:24–28
26. Vu A, Qian YQ, Stein A (2012) Porous electrode materials for lithium-ion batteries-how to prepare them and what makes them special. Adv Energy Mater 2:1056–1085
27. Balaji S, Vasuki R, Mutharasu D (2013) A feasibility study on SnO_2/$NiFe_2O_4$ nanocomposites as anodes for Li ion batteries. J Alloys Compd 54:25–31
28. Huang XH, Tu JP, Xia XH, Wang XL, Xiang JY, Zhang L, Zhou L (2009) Morphology effect on the electrochemical performance of NiO films as anodes for lithium ion batteries. J Power Sources 188: 588–591
29. Huang XH, Tu JP, Zhang B, Zhang CQ, Li Y, Yuan YF, Wu HM (2006) Electrochemical properties of NiO-Ni nanocomposite as anode material for lithium ion batteries. J Power Sources 161:541–544
30. Qiao H, Yao D, Cai YB, Huang FL, Wei QF (2013) One-pot synthesis and electrochemical property of MnO/C hybrid microspheres. Ionics 19:595–600